J. Phys.: Condens. Matter **21** (2009) 164212 (7pp) doi:10.1088/0953-8984/21/16/164212

Fermi surface reconstruction in high-T_c superconductors

Louis Taillefer

Canadian Institute for Advanced Research, Regroupement Québécois sur les Matériaux de Pointe, Département de Physique, Université de Sherbrooke, Sherbrooke, Canada

E-mail: Louis.Taillefer@USherbrooke.ca

Received 22 January 2009
Published 31 March 2009
Online at stacks.iop.org/JPhysCM/21/164212

Abstract

The recent observation of quantum oscillations in underdoped high-T_c superconductors, combined with their negative Hall coefficient at low temperature, reveals that the Fermi surface of hole-doped cuprates includes a small electron pocket. This strongly suggests that the large hole Fermi surface characteristic of the overdoped regime undergoes a reconstruction caused by the onset of some order which breaks translational symmetry. Here we consider the possibility that this order is 'stripe' order, a form of combined charge/spin modulation observed most clearly in materials like Eu-doped and Nd-doped LSCO ($La_{2-x}Sr_xCuO_4$). In these materials, the onset of stripe order coincides with major changes in transport properties, providing strong evidence that stripe order is indeed the cause of Fermi surface reconstruction. We identify the critical doping where this reconstruction occurs and show that the temperature dependence of transport coefficients at that doping is typical of metals at a quantum critical point. We discuss how the pseudogap phase may be a fluctuating precursor of the stripe-ordered phase.

(Some figures in this article are in colour only in the electronic version)

1. Phase diagram

The doping phase diagram of hole-doped cuprates is sketched in figure 1(a). With increased doping p, the materials go from being antiferromagnetic insulators at zero doping to more or less conventional metals at high doping. The overdoped metallic state is characterized by a single large hole Fermi surface whose volume contains $1 + p$ holes per Cu atom, as determined by angle-dependent magneto-resistance (ADMR) [1] and angle-resolved photoemission spectroscopy (ARPES) [2]. The low-temperature Hall coefficient R_H is positive and equal to $1/e(1 + p)$ [3], as expected for a single-band metal with a hole density $n = 1 + p$. The electrical resistivity $\rho(T)$ exhibits the standard T^2 temperature dependence of a Fermi liquid [4].

At intermediate doping, between the insulator and the metal, there is a central region of superconductivity, delineated by a critical temperature T_c which can rise to values of order 100 K. Above the maximal T_c, near optimal doping, the normal state is a 'strange metal', characterized by a resistivity which is linear in temperature instead of quadratic. In the midst of this strange-metal region, the enigmatic 'pseudogap phase' sets in, below a crossover temperature T^* where most physical properties undergo a smooth yet significant change [5].

Elucidating the nature of the pseudogap phase is key to understanding high-temperature superconductivity. Two main scenarios have been proposed [6]: fluctuating superconductivity—a precursor to the long-range coherence which sets in below T_c—versus some other ordered state. For hole-doped cuprates, a number of different types of order have been proposed, including 'stripe order' [7], d-density-wave order [8] and orbital currents [9]. In this paper, we review some recent transport measurements performed in magnetic fields high enough to suppress superconductivity and thus give access to the normal-state behaviour of hole-doped cuprates down to low temperature. These shed new light on the ground state of the pseudogap phase, raising hopes of finally unravelling this mysterious phenomenon.

2. Quantum oscillations

In 2007, quantum oscillations were finally observed in a high-T_c superconductor [10]. A key factor in the ability to detect these oscillations, whose amplitude decreases exponentially

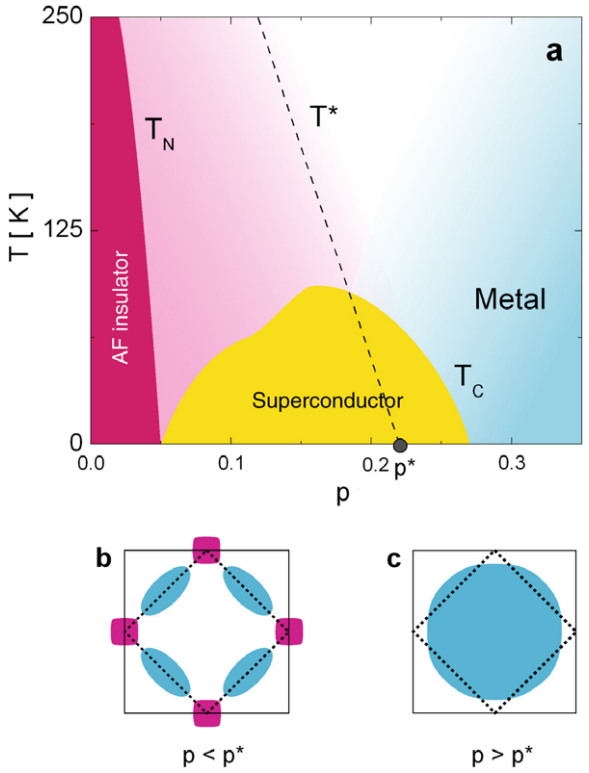

Figure 1. Phase diagram of hole-doped high-T_c superconductors. (a) Schematic doping dependence of the antiferromagnetic (T_N) and superconducting (T_c) transition temperatures and the pseudogap crossover temperature T^*. The fact that the large hole-like Fermi surface characteristic of the overdoped metallic state, sketched in panel (c), is modified in the underdoped region (see text) implies that there is a critical doping p^* where Fermi surface reconstruction occurs. (b) Schematic drawing of one possible reconstruction, that would result from an order with (π, π) wavevector, as in the antiferromagnetic state.

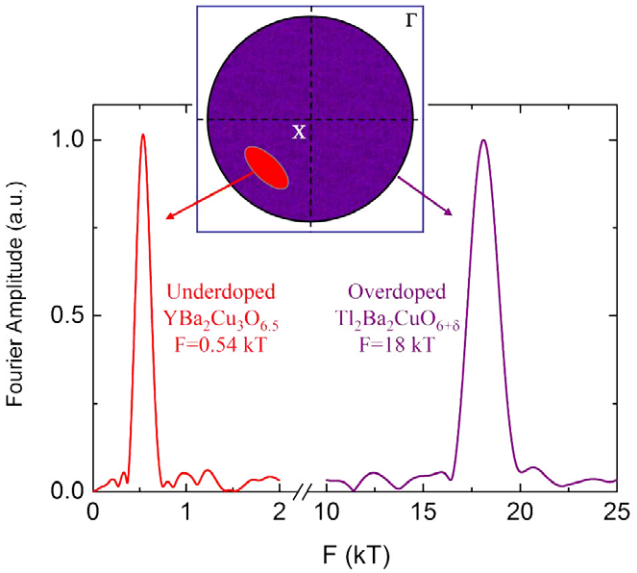

Figure 2. Fourier transform of the quantum oscillations detected in YBCO at $p = 0.1$ and Tl-2201 at $p \simeq 0.25$. Each reveals a single frequency F, but with vastly different values, as indicated. This shows that the Fermi surface in the underdoped regime includes a pocket which is much smaller than that in the overdoped regime, as sketched in the inset. Courtesy of Cyril Proust; reproduced from [13] with permission.

with increased disorder, was the high degree of ortho-II oxygen order in single crystals of $YBa_2Cu_3O_y$ (YBCO) [11]. Quantum oscillations result from the Landau quantization of states in a magnetic field and the orbiting motion of quasiparticles around the various pockets of the Fermi surface in a metal. Their very observation confirms the existence of a coherent closed Fermi surface and their frequency F is a direct measure of the Fermi surface area, via the relation $F = n\Phi_0$, where n is the carrier density enclosed by the particular Fermi surface associated with a given frequency, and Φ_0 is the quantum of flux.

First observed in the electrical resistance (both Hall and longitudinal; the Shubnikov–de Haas effect) [10], the same oscillations were soon also detected in the de Haas-van Alphen effect (magnetization) [12]. The Fourier transform of the oscillatory spectrum in $YBa_2Cu_3O_{6.5}$, reproduced in figure 2 (from [13]), reveals a single frequency at $F = 540$ T [10, 12]. In 2008, quantum oscillations were observed in strongly overdoped $Tl_2Ba_2CuO_{6+\delta}$ (Tl-2201), which also reveal a single frequency, but now at $F = 18$ kT [14] (see figure 2). This large value matches the area derived previously from ADMR and ARPES measurements on the same material at a similar doping and agrees with $n = 1 + p$.

The contrast between Tl-2201 at $p \approx 0.25$ and YBCO at $p = 0.1$ is dramatic: the Fermi surface area differs by a factor 30 (see figure 2). Note that the small pockets detected in underdoped YBCO are not a special feature of the band structure of that particular material, since similar quantum oscillations were observed in the stoichiometric underdoped cuprate $YBa_2Cu_4O_8$ [15, 16], whose band structure is significantly different [17]. Therefore, this transformation of the Fermi surface from large cylinder to small pockets is a robust signature of the pseudogap phase, which must occur at a $T = 0$ critical doping p^* somewhere between 0.1 and 0.25 (see figure 1).

3. Electron Fermi surface

A second important fact is that the low-frequency oscillations in $YBa_2Cu_3O_{6.5}$ and $YBa_2Cu_4O_8$ are observed on the background of a negative Hall coefficient R_H at low temperature [18] (figure 3(a)). As a function of temperature, $R_H(T)$ goes from small and positive at high temperature to large and negative as $T \to 0$ (figure 3(b)). Given that $R_H \sim 1/n$ and $F \sim n$, this is consistent with the transition from large to small Fermi surface revealed by quantum oscillations, but the fact that $R_H(T \to 0) < 0$ implies that the small Fermi surface seen in the underdoped regime must in fact be an electron-like pocket.

The emergence of an electron pocket in the Fermi surface of these hole-doped materials is of fundamental significance: it immediately suggests that the transformation of the Fermi surface is caused by the onset of a new periodicity, typically imposed by some density-wave order [19]. The simplest

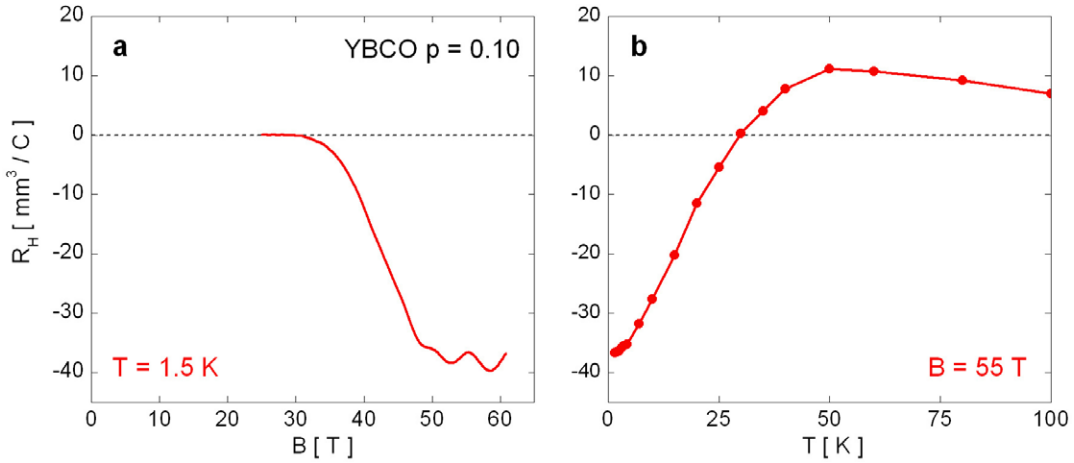

Figure 3. Hall coefficient in YBCO at $p = 0.1$, as a function of magnetic field at $T = 1.5$ K (left panel; (a)) and as a function of temperature at $B = 55$ T (right panel; (b)). The fact that quantum oscillations are observed on a large negative background implies that they arise from orbits around a closed electron-like Fermi surface pocket. Adapted from [18].

case to visualize is commensurate (π, π) antiferromagnetic order, which would cause the large hole-like Fermi surface of cuprates to be reconstructed into small hole and electron pockets [20], located respectively at $(\pi/2, \pi/2)$ and $(\pi, 0)$, as sketched in figure 1(b). Because d-density-wave order breaks translational symmetry in the same way, a similar reconstruction is produced [21]. However, a different reconstruction is expected for 'stripe order', a state with both charge and spin modulations, with wavevectors $(0, \pm 2\delta)$ and $(\frac{1}{2}, \frac{1}{2} \pm \delta)$, respectively [22]. In the case of commensurate anti-phase stripe order ($\delta = 1/8$), the Fermi surface is generically predicted to have hole pockets, electron pockets and quasi-1D open sheets [23], as sketched in figure 4. Note that quantum oscillations do not allow us to locate the position of the associated Fermi pockets in k-space, so the observed electron pocket can in principle be anywhere in the (reconstructed) Brillouin zone, and the three types of order just mentioned are *a priori* consistent with the evidence so far.

The Hall coefficient of YBCO at $p = 0.12$ is shown in figure 5(b) (from [18]). We see that $R_H(T)$ starts to drop below 100 K and changes sign at $T_0 = 70$ K [18]. We emphasize that this drop cannot be caused by a vortex (flux flow) contribution to the Hall effect because it is entirely independent of magnetic field, for fields ranging all the way from $B \approx 0$ to $B = 45$ T. In other words, T_0 is constant, while the superconducting transition temperature goes from $T_c = 66$ K at $B = 0$ to $T_c \approx 0$ at $B = 45$ T (see supplementary information in [18]), and is therefore a property of the normal state. This independence of T_0 on field also shows that the modification of the Fermi surface implied by the sign change in R_H is characteristic of the zero-field pseudogap phase, not some field-induced ordered state.

A drop in the normal-state $R_H(T)$ is a generic feature of hole-doped cuprates near $p = 1/8$, observed in $Bi_2La_{2-x}Ba_xCuO_{6+\delta}$ [24], $La_{2-x}Sr_xCuO_4$ (LSCO) [25], $La_{2-x}Ba_xCuO_4$ [26], Nd-doped LSCO (Nd–LSCO) [27] and Eu-doped LSCO (Eu–LSCO) [28], in addition to $YBa_2Cu_3O_y$ and $YBa_2Cu_4O_8$ [18]. The depth of the drop in a particular

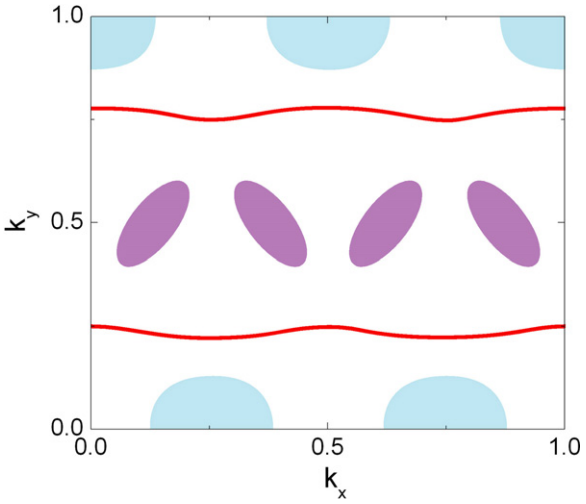

Figure 4. Calculated Fermi surface in the anti-phase stripe-ordered state of a hole-doped cuprate at $p = 1/8$, for a finite spin potential. Three types of Fermi surfaces are generically predicted: electron pockets (pale blue; along the edges), hole pockets (pink; in the center) and quasi-1D open sheets (red lines). Adapted from [23].

sample will depend on the relative mobility of electron-like and hole-like carriers. In figure 5(b), we compare YBCO and Eu–LSCO [29] at $p = 1/8$. The drops in $R_H(T)$ are so strikingly similar, it would be surprising if the underlying mechanism were not the same. Now, in Eu–LSCO, the drop in $R_H(T)$ coincides with the onset of charge 'stripe' order measured by resonant soft x-ray diffraction [30], as reproduced in figure 5(a). This is compelling evidence that stripe order causes a Fermi surface reconstruction which shows up as a pronounced change in the Hall coefficient.

4. Stripe order

In order to further investigate the impact of stripe order on the Fermi surface of cuprates, we have studied Nd–LSCO,

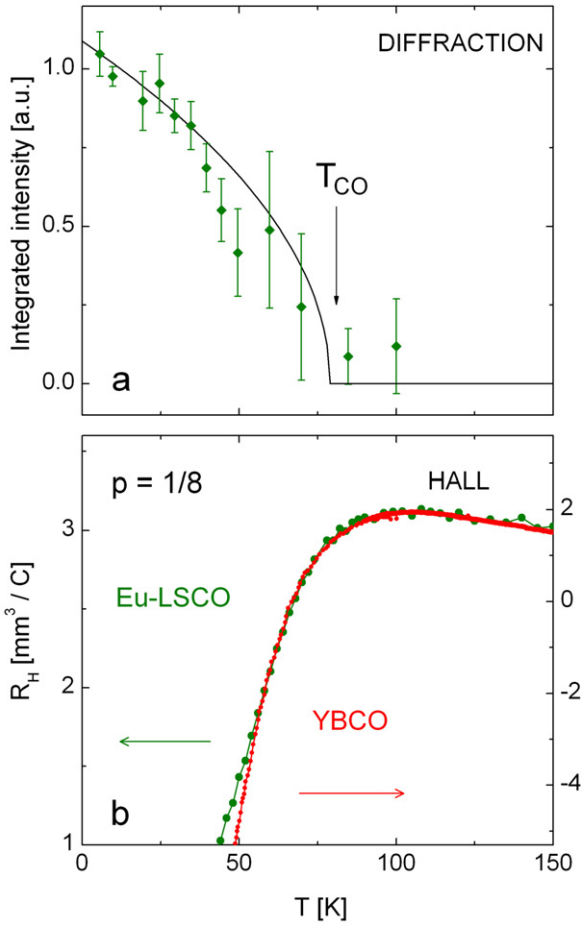

Figure 5. Stripe order and Hall coefficient in Eu–LSCO at $p = 1/8$. (a) Temperature dependence of charge order in Eu–LSCO at $p = 1/8$, as detected by resonant soft x-ray diffraction (data from [30]). (b) Hall coefficient versus temperature measured in $B = 15$ T for Eu–LSCO (green; left axis; data from [29]) and YBCO (red; right axis; data from [18]) at $p = 1/8$.

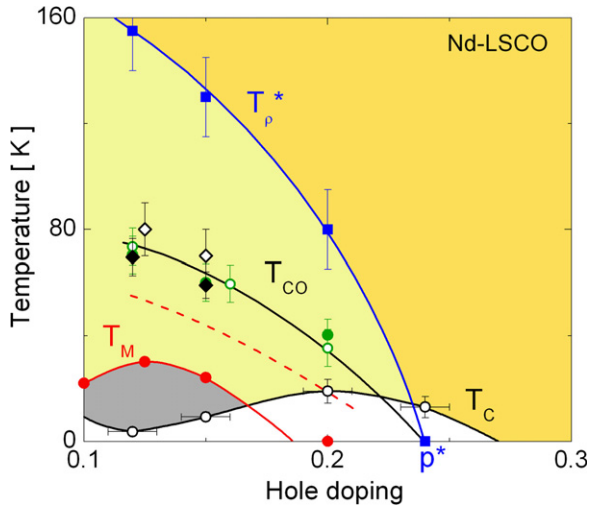

Figure 6. Temperature-doping phase diagram of Nd–LSCO showing the superconducting phase below T_c (open black circles) and the pseudogap region delineated by the crossover temperature T^*_ρ (blue squares). Also shown is the region where static magnetism is observed below T_M (full red circles) and charge order is detected below T_{CO} (black diamonds and green circles). These onset temperatures are respectively defined as the temperature below which: (1) the resistance is zero; (2) the in-plane resistivity $\rho(T)$ deviates from its linear dependence at high temperature; (3) an internal magnetic field is detected by zero-field muon spin relaxation (μSR); (4) charge order is detected by either x-ray diffraction or NQR. All lines are a guide to the eye. The red dashed line shows the onset of spin modulation as detected by neutron diffraction [39]. The blue line (T^*_ρ) above $p = 0.20$ is made to end at $p = 0.24$, thereby defining the critical doping where T^*_ρ goes to zero as $p^* = 0.24$. Experimentally, this point must lie in the range $0.20 < p^* \leqslant 0.24$, since $\rho(T)$ remains linear down to the lowest temperature at $p = 0.24$ [33]. T_M is obtained from the μSR measurements of [36]. The red line is made to end below $p = 0.20$, as no static magnetism was detected at $p = 0.20$ down to $T = 2$ K. T_{CO} is obtained from hard x-ray diffraction on Nd–LSCO (full black diamonds [31]) and from resonant soft x-ray diffraction on Eu–LSCO (open diamonds [30]). The onset of charge order has been found to coincide with the wipe-out anomaly in NQR, reproduced here from [32] for Nd–LSCO (closed green circles) and Eu–LSCO (open green circles).

a material isostructural to Eu–LSCO, which exhibits very similar charge and spin ordering. The onset of charge order in the two materials occurs at essentially the same temperature, T_{CO}, as a function of doping. Two measures of T_{CO}, obtained respectively from x-ray diffraction [30, 31] and nuclear quadrupole resonance (NQR) [32], are plotted in the phase diagram of figure 6. In particular, we have compared two samples of Nd–LSCO, respectively at $p = 0.20$ and 0.24 [33]. In figure 7, we show the in-plane resistivity $\rho(T)$ and Hall coefficient $R_H(T)$, from [33], and the Seebeck coefficient (or thermopower) S, plotted as S/T, from [34], as a function of temperature.

At $p = 0.24$, $R_H(T)$ is flat at low temperature (see figure 7(c)) and equal to the value expected of a single large cylinder containing $1 + p$ holes, namely $R_H = +1/e(1 + p)$, just as found in Tl-2201 at a similar doping [3]. The other two coefficients, $\rho(T)$ and S/T, are equally monotonic and featureless. By contrast, at $p = 0.20$, all three transport coefficients exhibit a pronounced upturn below 40 K, which shows that the Fermi surface has undergone a significant modification. These simultaneous upturns coincide with the onset of charge order detected by NQR at $T_{CO} = 40$ K [30], as reproduced in figure 7(a). So as in the case of Eu–LSCO at $p = 1/8$, there is little doubt that stripe order causes Fermi surface reconstruction in Nd-LSCO.

An intriguing difference is that $R_H(T)$ rises below T_{CO} at $p = 0.20$ (figure 7(c)), while it drops at $p = 1/8$ (figure 5(b)). If the drop in $R_H(T)$ near $p = 1/8$ is caused by a high-mobility electron pocket, then the rise at $p = 0.20$ suggests that this electron pocket is absent at higher doping. Calculations of the Hall coefficient in the stripe-ordered phase [35] reveal that a negative R_H requires a finite spin-stripe potential, the cause of a robust electron pocket in the Fermi surface [23] (as in figure 4). The observed evolution from a rise in R_H just below p^* to a drop in R_H (in some cases to negative values) near $p = 1/8$, may therefore reflect an increase in the spin-stripe potential relative to the charge-stripe potential. This would seem consistent with the fact that static spin order detected by muon spin relaxation, whose onset at T_M is plotted in figure 6, is absent at $p = 0.20$ and strongest at $p = 0.12$ [36].

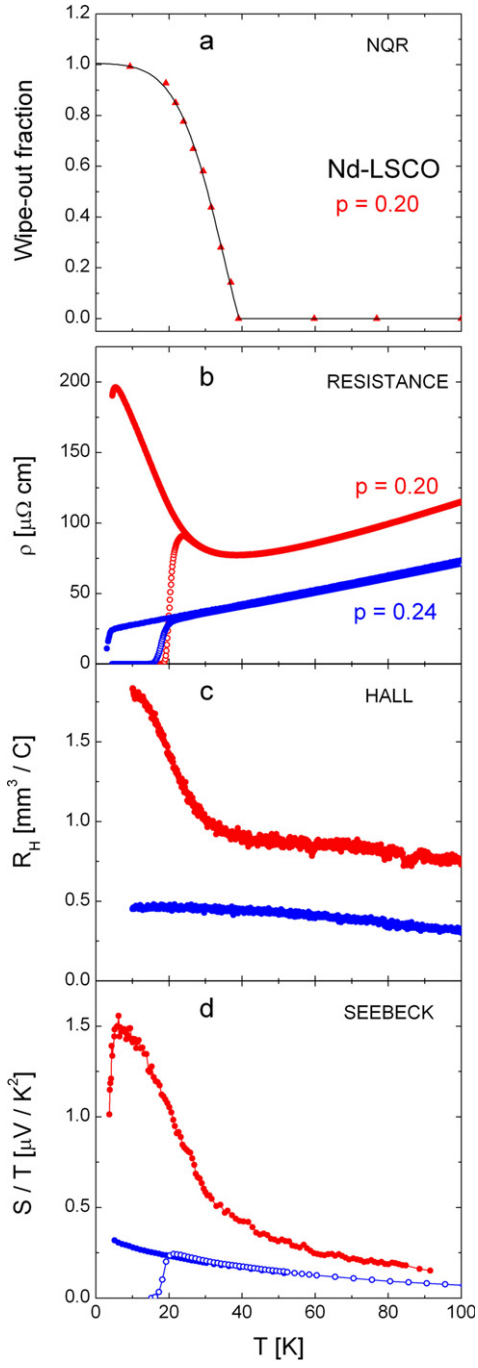

Figure 7. Stripe order and transport coefficients in Nd–LSCO. (a) Charge ordering in Nd–LSCO at $p = 0.20$, as measured by the loss of NQR intensity (adapted from [32]). At dopings $p = 0.12$ and 0.15 where both x-ray diffraction and NQR where measured on Nd–LSCO, the lost (or 'wipe-out') fraction of the intensity present at 100 K tracks the increase in the intensity of superlattice peaks detected with x-rays. At $p = 0.20$, the onset of charge order is $T_{CO} = 40 \pm 6$ K [32]. *Lower panels*: transport coefficients in two samples of Nd–LSCO, respectively with $p = 0.20$ (red; above) and at $p = 0.24$ (blue): (b) in-plane electrical resistivity ρ in a magnetic field $B = 0$ (open symbols) and 15 T (closed symbols) (adapted from [33]); (c) Hall coefficient R_H in 15 T (from [33]); (d) Seebeck coefficient S plotted as S/T for $B = 0$ (open symbols) and 15 T (closed symbols) (adapted from [34]). Note how at $p = 0.20$ all coefficients show a pronounced and simultaneous upturn starting at a temperature which coincides with the onset of charge order—strong evidence for a scenario of Fermi surface reconstruction by stripe order.

5. The pseudogap phase

What relation might there be between the stripe-ordered phase which sets in below T_{CO} and the mysterious pseudogap phase delineated by the higher crossover temperature T^*, sketched in figure 1 ? One way to define T^* is through the resistivity [5], as the temperature below which $\rho(T)$ deviates from its linear dependence at high temperature. A resistively-defined T^*, which we label T^*_ρ, was first reported for YBCO [37], where the deviation is downwards. In LSCO, however, the deviation is upwards [38], as indeed in Nd–LSCO [27, 33, 39]. The difference may simply reflect two limits: the clean limit, relevant for YBCO, where the loss of inelastic scattering caused by the opening of the pseudogap is more important than the loss in carrier density, and the dirty limit, relevant to LSCO and Nd–LSCO, where the reverse is true [33]. In figure 6, we plot T^*_ρ versus p for Nd–LSCO (from [33]). Both T_{CO} and T^*_ρ appear to end at the same critical point $p^* \approx 0.24$, and $T^*_\rho \approx 2T_{CO}$. The onset of spin modulation seen in neutron diffraction (dashed line in figure 6) also appears to end at p^* [39].

In this context, it seems natural to interpret the pseudogap phase as a fluctuating precursor of the long-range ordered state that sets in at lower temperature [40]. The onset of fluctuations at a temperature T^* well above T_{CO} may be understood from calculations which show quite generally that, for layered materials, precursors of the ordered state appear when the correlation length of the fluctuating order parameter exceeds the thermal de Broglie wavelength of the charge carriers [41]. Precursor features include a pseudogap and hot spots on the Fermi surface. Quantitative agreement between calculations on the Hubbard model at moderate coupling [42] and neutron diffraction measurements [43] confirm this interpretation in the case of electron-doped high-T_c superconductors.

6. Quantum critical point

The Fermi surface reconstruction in Nd–LSCO occurs between $p = 0.20$ and 0.24. The phase diagram in figure 6 suggests that at $T = 0$ it takes place at $p^* \approx 0.24$. Above this critical doping, the Fermi surface is in its pristine large hole-like state, and it is profoundly modified below p^*. While the value of p^* may be somewhat different in YBCO, quantum oscillations show that there must also be a $T = 0$ critical point in that material at which Fermi surface reconstruction occurs, somewhere above 0.1, and probably below 0.25. From an analysis of various physical properties, it has been proposed that $p^* \approx 0.19$ [44].

It is interesting to scrutinize the low-temperature properties of the metallic state at p^*. Close inspection reveals that $\rho(T)$ is linear down to the lowest temperature [33] and S/T exhibits a perfect $\log(1/T)$ dependence below 100 K [34]. This $\log(1/T)$ dependence of S/T is reminiscent of the $\log(1/T)$ dependence observed in C_e/T, the electronic specific heat divided by temperature, at the quantum critical point of various heavy-fermion metals [45]. The similarity with the antiferromagnetic compound $CeCu_{6-x}Au_x$ [46], for example, is remarkable (see [34]), both materials displaying

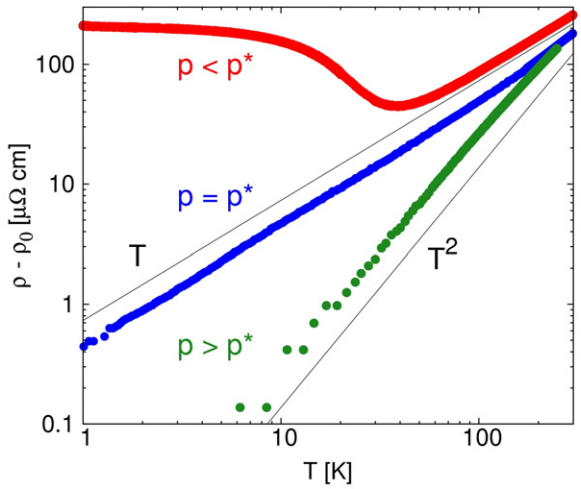

Figure 8. Three regimes of quantum criticality. Temperature dependent part of the resistivity, $\rho(T) - \rho_0$, versus log T for Nd–LSCO with $p = 0.20$ ($p < p^*$) and $p = 0.24$ ($p = p^*$), from [33], compared to that of LSCO with $p = 0.30$ ($p > p^*$), from [4]. ρ_0 is the value to which $\rho(T)$ extrapolates at $T = 0$; for Nd–LSCO at $p = 0.20$, the extrapolation is based only on data above 80 K. Taken from [34].

the three distinctive regimes of quantum criticality, whereby S/T and C_e/T are relatively flat in the Fermi-liquid state, logarithmically divergent at the critical point, and jump upon entering the ordered state.

This qualitative similarity suggests that p^* in Nd–LSCO is a quantum critical point at which a quantum phase transition occurs. This is reinforced by the resistivity behaviour, which also displays the three regimes characteristic of a quantum critical point, as shown in figure 8 (from [34]): quadratic in the Fermi-liquid state, linear at the critical point, and an upturn below that point.

There is also a strong similarity between Nd–LSCO and the electron-doped cuprate $Pr_{2-x}Ce_xCuO_4$ (PCCO), where the case for a quantum critical point is well established [47]. In the $T \to 0$ limit, both $R_H(T)$ and S/T in PCCO show an abrupt change as the doping x drops below the critical doping x_c, signalling a change in Fermi surface from a large hole cylinder to a combination of small electron and hole pockets [48, 49]. The two coefficients track each other, as equivalent measures of the effective carrier density [48]. At $x = x_c$, $\rho(T)$ is linear in temperature at low temperature [50]. These typical signatures of a quantum critical point have been attributed to the loss of antiferromagnetic order near x_c [43], and the quantum fluctuations thereof.

In a model of charge carriers on a three-dimensional Fermi surface scattered by two-dimensional antiferromagnetic spin fluctuations, transport properties near the magnetic quantum critical point are found to be dominated by 'hot spots', points on the Fermi surface connected by the ordering wavevector. In this case, calculations show that $\rho(T) \sim T$, $C_e/T \sim \log(1/T)$ and $S/T \sim \log(1/T)$ [51]. More generally, both $\rho(T) \sim T$ and $C_e/T \sim \log(1/T)$ follow naturally from a marginal Fermi-liquid phenomenology [52].

7. Conclusion

The low frequency of quantum oscillations and the drop in Hall coefficient to deeply negative values observed in YBCO near $p = 1/8$ demonstrate that the large hole Fermi surface of overdoped cuprates undergoes a profound reconstruction in the pseudogap phase. In the case of Eu–LSCO and Nd–LSCO, this reconstruction is clearly caused by the onset of stripe order. Given the striking similarity between YBCO and Eu–LSCO in the way $R_H(T)$ drops below 100 K at $p = 1/8$, it is tempting to invoke the same mechanism in YBCO. However, the lack of evidence for static stripe order in YBCO at $p = 1/8$ raises an interesting question: are fluctuating charge/spin modulations sufficient to alter the Fermi surface? This would point to a scenario where the pseudogap phase is a fluctuating precursor of a long-range stripe order that only sets in at lower temperature [7, 40, 53]. Further experimental and theoretical investigations are needed to answer this question and explore this scenario.

Acknowledgments

I wish to thank my collaborators on studies of the Fermi surface of cuprates: Luis Balicas, Doug Bonn, Olivier Cyr-Choinière, Ramzy Daou, Nicolas Doiron-Leyraud, Walter Hardy, Nigel Hussey, Francis Laliberté, David LeBoeuf, Shiyan Li, Ruixing Liang, Cyril Proust, Hidenori Takagi, and Jianshi Zhou. I also acknowledge stimulating discussions on this topic with Kamran Behnia, Sudip Chakravarty, Patrick Fournier, Richard Greene, Yong Baek Kim, Hae-Young Kee, Steve Kivelson, Gilbert Lonzarich, Andrew Millis, Michael Norman, Subir Sachdev, Todadri Senthil and André-Marie Tremblay. I would like to thank Louise Brisson for her constant support and Jacques Corbin for his help with several experiments. I acknowledge the long-term support of the Canadian Institute for Advanced Research and funding from NSERC, FQRNT, CFI and a Canada Research Chair.

References

[1] Hussey N E *et al* 2003 *Nature* **425** 814
[2] Platé M *et al* 2005 *Phys. Rev. Lett.* **95** 077001
[3] Mackenzie A P *et al* 1996 *Phys. Rev.* B **53** 5848
[4] Nakamae S *et al* 2003 *Phys. Rev.* B **68** 100502
[5] Timusk T and Statt B 1999 *Rep. Prog. Phys.* **62** 61
[6] Norman M R, Pines D and Kallin C 2005 *Adv. Phys.* **54** 715
[7] Kivelson S A *et al* 2003 *Rev. Mod. Phys.* **75** 1201
[8] Chakravarty S *et al* 1997 *Phys. Rev.* B **55** 14554
[9] Varma C M 2003 *Phys. Rev.* B **68** 100502
[10] Doiron-Leyraud N *et al* 2007 *Nature* **447** 565
[11] Liang R *et al* 2006 *Phys. Rev.* B **73** 180505
[12] Jaudet C *et al* 2008 *Phys. Rev. Lett.* **100** 187005
[13] Jaudet C *et al* 2009 *Physica* B **404** 354–6
[14] Vignolle B *et al* 2008 *Nature* **455** 952
[15] Yelland E *et al* 2008 *Phys. Rev. Lett.* **100** 047003
[16] Bangura A F *et al* 2008 *Phys. Rev. Lett.* **100** 047004
[17] Carrington A and Yelland E A 2007 *Phys. Rev.* B **76** 140508
[18] LeBoeuf D *et al* 2007 *Nature* **450** 533
[19] Chakravarty S 2008 *Science* **319** 735
[20] Chubukov A V and Morr D K 1997 *Phys. Rep.* **288** 355
[21] Chakravarty S and Kee H Y 2008 *Proc. Natl Acad. Sci.* **105** 8835
[22] Tranquada J M *et al* 1995 *Nature* **375** 561

[23] Millis A J and Norman M R 2007 *Phys. Rev.* B **76** 220503
[24] Balakirev F F *et al* 2003 *Nature* **424** 912
[25] Balakirev F F *et al* 2009 *Phys. Rev. Lett.* **102** 017004
[26] Adachi T *et al* 2001 *Phys. Rev.* B **64** 144524
[27] Nakamura Y and Uchida S 1992 *Phys. Rev.* B **46** 5841
[28] Takeshita N *et al* 2004 *J. Phys. Soc. Japan* **73** 1123
[29] Cyr-Choinière O *et al* 2009 in preparation
[30] Fink J *et al* 2008 arXiv:0805.4352 [cond-mat]
[31] Niemoller T *et al* 1999 *Eur. Phys. J.* B **12** 509
[32] Hunt A W *et al* 2001 *Phys. Rev.* B **64** 134525
[33] Daou R *et al* 2009 *Nat. Phys.* **5** 31
[34] Daou R *et al* 2008 arXiv:0810.4280 [cond-mat]
[35] Lin J and Millis A J 2008 *Phys. Rev.* B **78** 115108
[36] Nachumi B *et al* 1998 *Phys. Rev.* B **58** 8760
[37] Ito T *et al* 1993 *Phys. Rev. Lett.* **70** 3995
[38] Ando Y *et al* 2004 *Phys. Rev. Lett.* **93** 267001
[39] Ichikawa N *et al* 2000 *Phys. Rev. Lett.* **85** 1738
[40] Kivelson S A, Fradkin E and Emery V J 1998 *Nature* **393** 551
[41] Vilk Y and Tremblay A M S 1997 *J. Physique* I **7** 1309
[42] Kyung B *et al* 2004 *Phys. Rev. Lett.* **93** 147004
[43] Motoyama E M *et al* 2007 *Nature* **445** 186
[44] Tallon J L and Loram J W 2001 *Physica* C **349** 53
[45] v Löhneysen H *et al* 2007 *Rev. Mod. Phys.* **79** 1015
[46] v Löhneysen H *et al* 1994 *Phys. Rev. Lett.* **72** 3262
[47] Dagan Y *et al* 2004 *Phys. Rev. Lett.* **92** 167001
[48] Li P *et al* 2007 *Phys. Rev.* B **75** 020506
[49] Lin J and Millis A J 2005 *Phys. Rev.* B **72** 214506
[50] Fournier P *et al* 1998 *Phys. Rev. Lett.* **81** 4720
[51] Paul I and Kotliar G 2001 *Phys. Rev.* B **64** 184414
[52] Varma C M *et al* 1989 *Phys. Rev. Lett.* **63** 1996
[53] Hinkov V *et al* 2008 *Science* **319** 597